Dalton Transactions

PAPER

View Article Online
View Journal | View Issue

Cite this: *Dalton Trans.*, 2014, **43**, 4163

One-step replication and enhanced catalytic activity for cathodic oxygen reduction of the mesostructured Co_3O_4/carbon composites†

Yongxia Wang,[a,b] Xiangzhi Cui,[b] Lisong Chen,[b] Chenyang Wei,[b] Fangming Cui,[c] Heliang Yao,[b] Jianlin Shi*[b] and Yongsheng Li*[a]

Received 12th November 2013,
Accepted 5th December 2013

DOI: 10.1039/c3dt53192a

www.rsc.org/dalton

Mesostructured Co_3O_4/C composites of high surface area have been synthesized *via* a one-step replica route by co-nanocasting cobalt and carbon precursors into mesoporous silica, in which the Co_3O_4 nanoparticles are homogeneously dispersed in the mesoporous structure of carbon substrates. The mesostructured composites showed relatively high catalytic activities for oxygen reduction reaction (ORR), and that with a Co loading content of 4.3 at% exhibited the best electrochemical performance for ORR. The relatively high catalytic activity is attributed to the effects of the redox couples (Co^{3+}/Co^{2+}) together with the contribution from the conductive mesoporous carbon substrate.

Introduction

Oxygen reduction reaction (ORR) is one of the fundamental reactions taking place on the cathode catalytic surface of H_2–O_2 fuel cells,[1,2] such as proton exchange membrane fuel cells (PEMFCs), which is so important that numerous efforts have been devoted to developing high performance while cost-effective cathode catalysts for ORR. Unfortunately, the present cathode catalysts in PEMFCs still face a number of problems and challenges. On the one hand, compared with a rather fast oxidization of hydrogen that produces a proton and an electron at the anode, the sluggish ORR is a main challenge for developing fuel cells of high enough performance and efficiency for commercial applications. On the other hand, the high cost and limited supply of the precious Pt-based catalysts, the most successful electrocatalysts for ORR up to now, greatly hinder their large-scale commercial applications.[3] Consequently, it is highly desirable to develop highly active cathode catalysts with as small as possible an amount of Pt or even non-precious metal catalysts. Bashyam and Lefèvre *et al.* are the pioneers in developing fuel cell technology using non-precious metal catalysts for ORR,[4,5] which has aroused great interest in searching for novel, highly active and stable non-precious metal catalysts over the past few decades,[6–9] in particular the non-precious metal-containing carbon nanostructured catalysts for ORR.[10–13]

Among the non-precious metal electro-catalysts for ORR, Co_3O_4 has been widely investigated as alternative catalysts in terms of their low cost, moderate electrical resistance and environmental friendliness, which demonstrates promising catalytic activity and durability in alkaline or acidic media.[14–17] However, Co_3O_4 is a p-type semiconductor, and the use of conductive substrates is necessary to elevate the electron conductivity and improve the electrochemical properties for ORR, among which, carbonaceous materials have been suggested as possible electrocatalyst supports attributing to their high mechanical strength, excellent electronic conductivity as well as chemical stability, such as Vulcan XC72, carbon nanotubes, graphene, mesoporous carbon, and so on.[18–23]

Mesoporous materials have been paid much attention in various application fields, such as catalysis, fine chemical engineering, drug delivery system, separation and adsorption, thanks to their high specific surface areas, pore volumes, controlled pore sizes and size distributions in their extensive mesoporosities, and so on.[24–28] The interconnected pore network of the mesoporous carbon benefits the diffusion of ORR-related molecules and dispersion of guest species, while the carbonaceous framework plays a role in electron conduction during ORR, both of which favors the enhancement of the electrochemical catalytic activity. However, up to now, the

[a]*Laboratory of Low-Dimensional Materials Chemistry, Key Laboratory for Ultrafine Materials of Ministry of Education, School of Materials Science and Engineering, East China University of Science and Technology, Shanghai 200237, China. E-mail: ysli@ecust.edu.cn*

[b]*The State Key Laboratory of High Performance Ceramics and Superfine Microstructures, Shanghai Institute of Ceramics, Chinese Academy of Sciences, Shanghai 200050, China. E-mail: jlshi@mail.sic.ac.cn; Fax: +86 21 52413122; Tel: +86 21 52412712*

[c]*Qian Xuesen Laboratory of Space Technology, China Academy of Space Technology, Beijing 100094, China*

†Electronic supplementary information (ESI) available: Pore structure parameters, XPS, CV curves, RDE voltammetry curves. See DOI: 10.1039/c3dt53192a

reported methodologies of preparing Co_3O_4/C composites were relatively complicated, which mainly involved two major steps of the carbon preparation with varied morphologies and the post-loading of the Co_3O_4 nanoparticles onto/into pre-obtained carbonaceous substrates.[18,29–31] Additionally, no reports can be found on the synthesis and the ORR performances of the mesostructured Co_3O_4/C composites prepared by a one-step process. Herein, we demonstrate the synthesis of a mesostructured Co_3O_4/C composite *via* a simple one-step replication route in which cobalt and carbon precursors were co-nanocasted into the pore network of a mesoporous silica template. The resultant composites show homogeneous dispersion of Co_3O_4 nanoparticles in a mesoporous network of the carbon substrates, and highly efficient performances in ORR.

Experimental

Synthesis of mesostructured Co_3O_4/C composites

The as-prepared mesoporous silica (KIT-6) following the procedure reported by Ryoo *et al.*[32] were used as a hard template for the preparation of mesostructured Co_3O_4/C composites. The typical synthesis procedure is as follows: different amounts of cobaltous acetate ($Co(C_2H_3O_2)_2$) and 1.5 mL furfuralcohol were dissolved in ethanol solvent. The above mixed solution was co-casted into 1.0 g as-prepared KIT-6 by a wetness impregnation technique. After the solvent evaporated, the precursors@silica composite was calcined at 1023 K for 4 h with a heating rate of 2 K min^{-1} in pure N_2. The silica template was finally removed by treating in 2 M NaOH solution at 353 K. These template-free Co_3O_4/C composites were collected by centrifugation and washed with distilled water and ethanol, and then dried at 353 K. The mesostructured Co_3O_4/C composites were named as 1-Co_3O_4/C, 2-Co_3O_4/C and 3-Co_3O_4/C, corresponding to the Co loading amounts of 1.1, 4.3 and 11.4 at%, respectively. For comparison, the mesoporous Co_3O_4 and carbon were also synthesized *via* the same process as that described above.

Characterization

The powder X-ray diffraction (XRD) patterns of the as-prepared samples were recorded on a Rigaku D/Max-2550 V X-ray diffractometer with a Cu Kα radiation target (40 kV, 40 mA). The morphology of the mesostructured Co_3O_4/C composites were observed using transmission electron microscopy (TEM) (a JEOL 200CX electron microscope operating at 160 kV). Raman spectra were recorded on a Micro-Raman spectrometer (Jobin Yvon HR800 UV) using an Ar ion laser (excitation wavelength: 514.5 nm). The N_2 sorption measurements were performed using Micromeritics TriStar 3000 at 77 K, and the specific surface area and pore size distributions were calculated using the Brunauer–Emmett–Teller (BET) and Barrett–Joyner–Halenda (BJH) methods, respectively.

Electrochemical experiments were performed on CHI 660E electrochemical workstation (CH Instrument, Inc.) with a standard three-electrode cell. Glassy carbon disks of 6 mm diameter (0.283 cm^2) served as substrate for the catalysts. Catalyst ink with 5 mg mL^{-1} (ethanol–water = 1 : 1, volume scale) and 25 μL Nafion solution (5%) was dispersed ultrasonically, and a 20 μL aliquot was transferred onto the glassy carbon substrate, yielding a catalyst loading level of 0.35 mg cm^{-2}. A platinum wire and Ag/AgCl (3 M KCl) were used as counter and reference electrodes, respectively. O_2-saturated 0.5 M H_2SO_4 solution was used as electrolyte for electrochemical measurements. The catalysts were characterized by a cyclic voltammetry (CV) test at room temperature. An electrode tip (ALS, RRDE-3A Operation Manual) was used for the rotating disk electrode (RDE) measurements, and glassy carbon disks of 4 mm diameter served as substrate for the catalyst materials. The kinetic parameters can be analyzed on the basis of the Koutecky–Levich equations:

$$\frac{1}{J} = \frac{1}{J_L} + \frac{1}{J_K} = \frac{1}{B\omega^{1/2}} + \frac{1}{J_K}$$

$$B = 0.62nFC_0(D_0)^{2/3}\nu^{-1/6}$$

$$J_K = nF\kappa C_0$$

in which J is the measured current density, J_K and J_L are the kinetic and diffusion-limiting current densities, ω is the rotation rate in rpm, n is the overall number of electrons transferred in oxygen reduction, F is the Faraday constant (F = 96 485 C mol^{-1}), C_0 is the bulk concentration of O_2 ($C_0 = 1.3 \times 10^{-6}$ mol cm^{-3}), D_0 is the diffusion coefficient of O_2 in the bulk solution ($D_0 = 1.7 \times 10^{-5}$ cm^2 s^{-1}), ν is the kinematic viscosity of the solution (0.01 cm^2 s^{-1}), k is the electron-transfer rate constant. The value of the electron transfer rate (n) can be obtained from the slope of the Koutecky–Levich plots (J^{-1} *vs.* $\omega^{-1/2}$).

The surface and/or lattice oxygen reduction behaviors of the obtained mesostructured Co_3O_4/C composites were explored using the temperature-programmed reduction of the hydrogen (H_2-TPR) technique in a temperature range from 293 to 1073 K on the TCD-GC analyzer. Typically, 50 mg of sample placed in glass tube was first thermally treated under a He flow at 923 K for 30 min at a rate of 10 K min^{-1}, and then cooled down to room temperature. Afterwards, 10% H_2 in Ar was introduced into the glass tube with a flow rate of 25 ml min^{-1} for the TPR experiment.

Results and discussion

XRD patterns of the as-prepared mesoporous Co_3O_4 and mesostructured Co_3O_4/C composites are shown in Fig. 1A, and all peaks can be well indexed to those of Co_3O_4 crystalline phase (JCPDS no. 42-1467). It can also be seen that the peak intensities of all Co_3O_4/C composites are relatively weak and broadened compared to those of the mesoporous Co_3O_4, indicating the diminished nanocrystalline size of Co_3O_4 particles after loading in the mesoporous carbon substrates. Fig. 1B and the inset give the small-angle XRD patterns of the as-prepared samples and silica template, respectively. The silica template

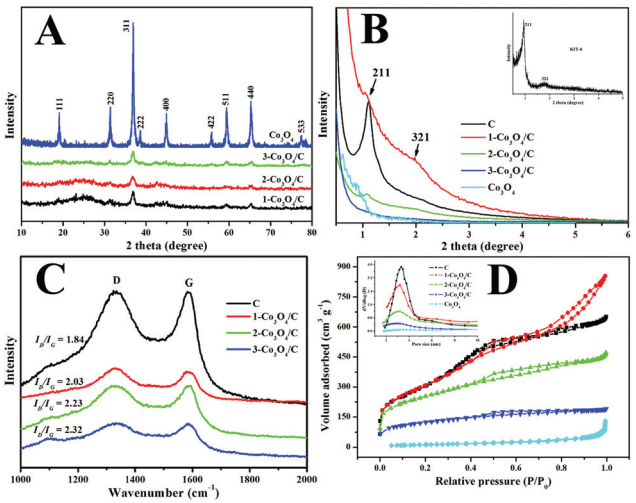

Fig. 1 Wide-angle and small-angle XRD patterns of the mesostructured Co_3O_4/C composites (A and B), the inset in B is the small-angle XRD pattern of the silica template; Raman spectra of the composites (C); N_2 sorption isotherms of the composites (D), the insets in (D) is the corresponding BJH pore size distribution.

exhibits well-resolved small angle peaks, and one characteristic diffraction peak (211) can be detected for the pure mesoporous carbon and Co_3O_4, indicating that the ordered pore structure can be reserved for the samples after silica template removal. The diffraction peaks of the Co_3O_4/C composites in the small angle region become less significant at the increased Co_3O_4 loading contents, indicating that the loading of Co_3O_4 nanoparticles will lead to partial damage of the mesopore ordering of the mesoporous carbon substrate during the co-nanocasting process. Moreover, the loaded Co_3O_4 may affect the microstructure of the carbon substrate as shown in the Raman spectra (Fig. 1C). The spectra show two bands at 1355 (D) and 1590 (G) cm^{-1}, and the I_D/I_G of the composites increases with an increase of the Co_3O_4 loading content, attributable to the defects and disorder of the carbon after loading of the Co_3O_4.

N_2 adsorption–desorption isotherms and the corresponding BJH pore size distribution curves of the obtained samples are shown in Fig. 1D. All samples show a type-IV isotherm with hysteresis loops located in the relative pressure range of 0.5–1.0, which is characteristic of mesoporous materials. The pore structure parameters of all samples are listed in Table S1,† and the specific surface area decreases gradually with increasing loading content of Co_3O_4, while all of the as-prepared mesoporous Co_3O_4/C composites show almost identical pore size distribution (about 3 nm). The Co contents from the XPS (Fig. S1†) were determined to be 1.1, 4.3 and 11.4 at%, corresponding to the as-prepared mesostructured 1-Co_3O_4/C, 2-Co_3O_4/C, and 3-Co_3O_4/C composites, respectively.

Fig. 2A and B give the TEM images of the mesoporous carbon and Co_3O_4, respectively, and it can be seen that both of the samples showed an ordered mesostructure after the removal of the silica template. Fig. 2C, D and E are the typical TEM images of 1-Co_3O_4/C, 2-Co_3O_4/C, and 3-Co_3O_4/C, respectively, which shows the homogenous dispersions of Co_3O_4

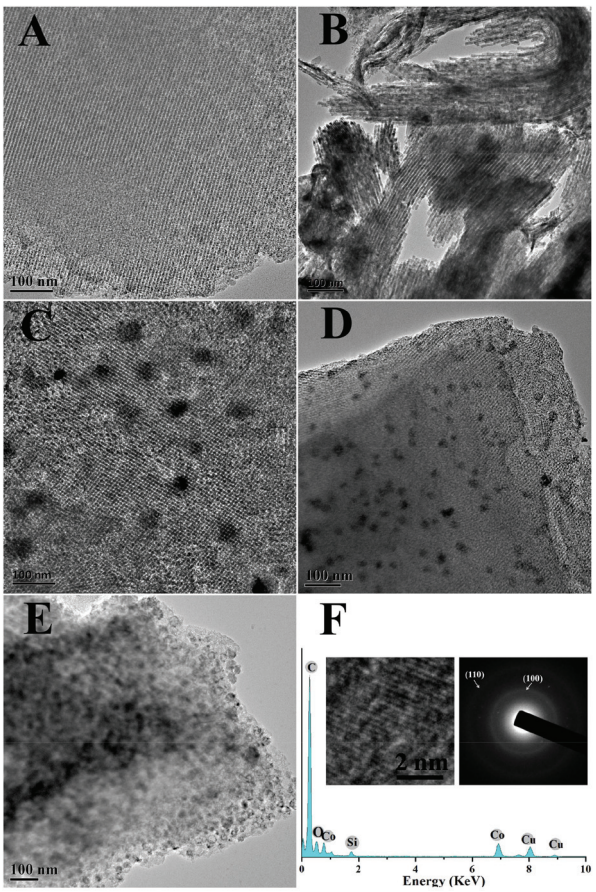

Fig. 2 TEM images of mesoporous carbon (A), Co_3O_4 (B), 1-Co_3O_4/C (C), 2-Co_3O_4/C (D), 3-Co_3O_4/C (E); EDS pattern of mesostructured 1-Co_3O_4/C (F), and the left and right insets in F are the corresponding HRTEM image and SAED pattern of the 1-Co_3O_4/C.

nanoparticles in/on the mesoporous carbon substrates. Moreover, with the increase of the Co_3O_4 loading content, the pore structure ordering of the Co_3O_4/C composites deteriorated gradually, which corresponds to the variation of their surface areas. The EDS of the mesostructured 1-Co_3O_4/C composite (Fig. 2D) also proves the successful loading of Co_3O_4 in the mesoporous carbon substrates in which the signals of Co and O can be readily detected. Additionally, a very weak Si signal can be distinguished, suggesting a trace amount of Si remained due to the strong interaction between silica and the obtained sample as also found by others.[33,34] The left inset in Fig. 2F is the HRTEM image of 1-Co_3O_4/C, and the (311) plane with a lattice space of 0.244 nm is observed for Co_3O_4 nanoparticles, indicating the crystalline character of Co_3O_4 in mesoporous carbon substrates. Meanwhile, the selected area electron diffraction (SAED) pattern (the right inset in Fig. 2F) shows clear evidence of a certain degree of graphitic structure of the mesoporous carbon substrates.

The electrochemical catalytic activities for oxygen reduction reaction (ORR) of the obtained mesostructured Co_3O_4/C composites were examined using cyclic voltammetry (CV) in O_2-saturated 0.5 M H_2SO_4. Fig. 3A gives the CV curves of the

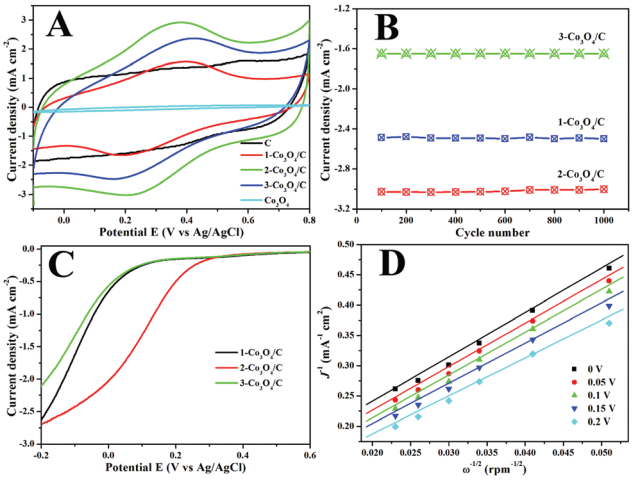

Fig. 3 CV curves of the mesostructured Co_3O_4/C composites in O_2-saturated 0.5 M H_2SO_4, ν = 50 mV s^{-1} (A); plots of current density *vs.* cycle number of the composites for oxygen reduction (B); RDE voltammetry curves of the composites for oxygen reduction obtained at 1600 rpm in O_2-saturated 0.5 M H_2SO_4, ν = 2 mV s^{-1} (C); Koutecky–Levich plots of 2-Co_3O_4/C in O_2-saturated 0.5 M H_2SO_4 for oxygen reduction at varied potentials (D).

composites under a scanning rate of 50 mV s^{-1}, and clear redox peaks can be observed for all of the Co_3O_4/C composites. However, the pure mesoporous Co_3O_4 and pure mesoporous carbon shows no redox peaks for ORR, indicating that neither mesoporous Co_3O_4 nor carbon is a satisfactory catalyst for oxygen reduction. Similar results have also been reported by Dai *et al.* that Co_3O_4 or graphene oxide alone has little catalytic activity, while the hybrid material of Co_3O_4 nanocrystals grown on reduced graphene oxide exhibits an unexpected, surprisingly high ORR activity.[18] Additionally, the mesostructured 2-Co_3O_4/C composites (Co content of 4.3 at%) show the highest ORR catalytic performance among the mesostructured Co_3O_4/C composites. This result indicates that the moderate Co_3O_4 loading favors the enhanced catalytic ORR activity of the catalysts, while over-high or over-low amounts of Co_3O_4 dispersions may lead to decreased activities in ORR. Additionally, though the reduction potential of the mesostructured 2-Co_3O_4/C composite (0.22 V) is lower than that of the standard E-TEK cathode catalysts 40% Pt/C (0.57 V) (Fig. S2A†), the maximum reduction current density of the 2-Co_3O_4/C about 3.0 mA cm^{-2} is similar to that of the Pt/C (about 2.6 mA cm^{-2}), indicating that the mesostructured 2-Co_3O_4/C composite is a good catalyst candidate for ORR. The peak current of the synthesized catalysts are also higher than most of the cobalt-based catalysts.[35,36] Fig. 3B gives the plots of current density of the Co_3O_4/C composites *versus* the cycle number, and the current density of all the catalysts can retain their initial current densities after several hundred or even one thousand cycles, indicating the high redox cycling stability. The current density *versus* time curves (Fig. S2B†) of the catalysts also exhibit the high ORR stability. Meanwhile, the CV curves of the mesostructured Co_3O_4/C composites after being cycled 1000 times for ORR are shown in Fig. S2(C–D).†

Linear sweep voltammetry with a rotating disk electrode (RDE) were further employed to study the ORR activity and kinetics of the composites. Fig. 3C shows the ORR polarization curves obtained at a rotation rate of 1600 rpm, and the onset potential for 2-Co_3O_4/C was detected to be 0.33 V, whereas it was 0.14 V for 1-Co_3O_4/C and 3-Co_3O_4/C. The half wave potential of 2-Co_3O_4/C is at 0.06 V, while the other two composites give a much more negative half wave potential at −0.1 V. The results from the polarization curves further prove that the 2-Co_3O_4/C has higher catalytic activity than the two others. To obtain a deeper insight into the electron transfer kinetics of mesostructured Co_3O_4/C composites during the ORR, typical RDE polarization behaviors of the composites and 40% Pt/C were investigated at different rotating rates (Fig. S3A†). The corresponding Koutecky–Levich plots (J^{-1} *vs.* $\omega^{-1/2}$) of 2-Co_3O_4/C at varied electrode potentials show excellent linearities (Fig. 3D), and the slopes remain approximately constant over the potential range from 0 to 0.2 V, indicating a similar electron-transfer number per O_2 molecule involved in the O_2 reduction. The values of n are around 3.8 in the full range of potential employed, indicating that the ORR process on the obtained 2-Co_3O_4/C may undergo a $4e^-$ combined pathway.

Fig. 4A shows the H_2-TPR profiles of the mesoporous Co_3O_4 and mesostructured Co_3O_4/C composites. From the H_2-TPR profile of the mesoporous Co_3O_4, two major successive steps were observed at about 573 and 633 K, corresponding to the reductions of Co^{3+} to Co^{2+}, and Co^{2+} to Co^0, respectively. However, compared with the mesoporous Co_3O_4, the two reduction steps of the mesostructured Co_3O_4/C composites shift to higher temperatures, and the peak areas become much smaller than that of the pure mesoporous Co_3O_4, most probably due to the low crystallinity and low amounts of the Co_3O_4 nanoparticles highly dispersed in the mesoporous carbon substrates (Fig. 1A, Table S1†). As expected, the peak area of the mesostructured Co_3O_4/C composites increases gradually from

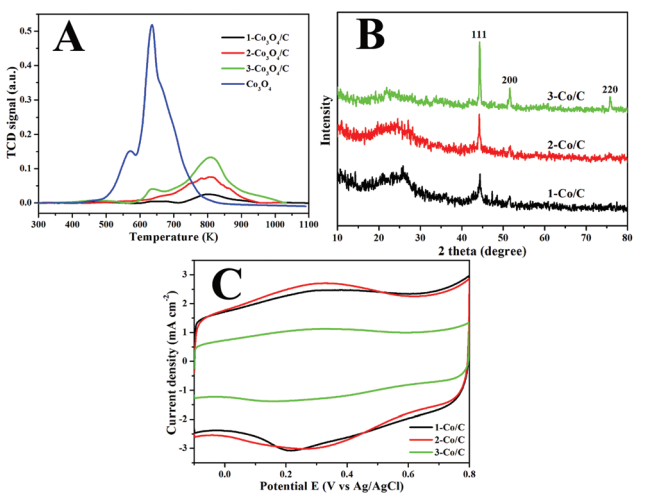

Fig. 4 H_2-TPR profiles of the mesostructured Co_3O_4/C composites (A); wide-angle XRD patterns of the mesostructured Co/C composites after heat treatment under 10% H_2/Ar (B); CV curves of the mesostructured Co/C composites in O_2-saturated 0.5 M H_2SO_4, ν = 50 mV s^{-1}.

1-Co_3O_4/C to 3-Co_3O_4/C, attributing to the increased Co_3O_4 contents. To confirm the total reduction of Co_3O_4 to Co, XRD patterns of the samples after H_2-TPR tests were recorded (Fig. 4B), and the results clearly show the XRD patterns of metal Co peaks at 2θ = 44.2°, 51.5° and 75.9°, corresponding to (111), (200) and (220) lattice planes, respectively (JCPDS no. 15-0806). No other peaks can be observed, indicating that the Co_3O_4 nanoparticles have been totally reduced to metal Co.

In order to further investigate the electrochemical catalytic activity of the Co_3O_4/C, the electrochemical tests of the corresponding mesostructured Co/C composites obtained after H_2 reduction were performed using CV measurements in O_2-saturated 0.5 M H_2SO_4. The CV curves of the Co/C composites with different Co loading contents are given in Fig. 4C. It can be seen that, besides a very weak redox peak for 1-Co/C, no redox peaks can be detected for other two mesostructured Co/C composites, suggesting that insignificant or negligible electrochemical ORR activities of the Co/C samples.

According to the electrochemical ORR properties of the mesoporous Co_3O_4 and carbon, mesostructured Co_3O_4/C and Co/C composites, it is understood that Co_3O_4 should be the active species responsible for the electrochemical activity for oxygen reduction. To have a clear understanding of the mesostructured Co_3O_4/C composites for the oxygen reduction process, a possible mechanism is proposed for the oxygen reduction by mesostructured Co_3O_4/C composites as shown schematically in Scheme 1. On the one hand, the conductivity of the carbon substrate can provide electron transfer channels to compensate for the weak conductivity of Co_3O_4 nanoparticles. On the other hand, the relatively high catalytic activity for ORR of the mesostructured Co_3O_4/C composite compared with the corresponding Co/C indicates that the Co_3O_4 nanoparticles as the main active species play an important role in oxygen reduction. The relatively high catalytic activity of mesostructured Co_3O_4/C may be attributed to the Co^{3+}/Co^{2+} redox couples, by means of which the O_2 molecules are decomposed into O_2^-/O^{2-} species. Additionally, the pore framework of the mesoporous carbon may benefit the diffusions of ORR related species and the enhancement of the catalytic activity.

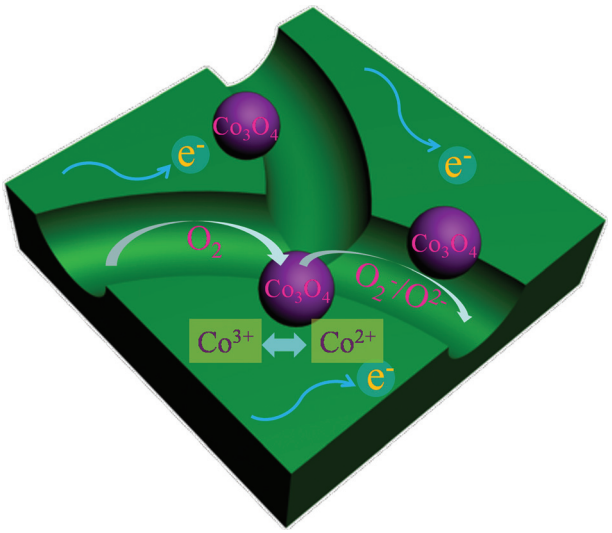

Scheme 1 Schematic illustration of mesostructured Co_3O_4/C composites for oxygen reduction. The mesoporous carbon substrates act as the electron transferred media and provide a channel for the diffusion of ORR related species and the enhancement of the catalytic activity. O_2 molecules diffused to the surface of Co_3O_4, are decomposed into O_2^-/O^{2-} species by means of the Co^{3+}/Co^{2+} redox couple.

Conclusions

In summary, the mesostructured Co_3O_4/C composites with Co_3O_4 nanoparticles homogeneously dispersed into mesoporous carbon substrate, are applicable noble metal-free catalytic candidates for oxygen reduction with relatively high catalytic activity and durability. 2-Co_3O_4/C with a Co loading content of 4.3 at% shows the highest electrochemical activity, and a $4e^-$ process is proposed as the main pathway for oxygen reduction. Moreover, the relatively high catalytic activity of the mesostructured Co_3O_4/C composites is mainly attributed to the redox couples (Co^{3+}/Co^{2+}) in Co_3O_4 nanoparticles, high conductivity of the carbon substrate and the mesoporous diffusion channels offered by the mesostructure of the composite catalysts for the ORR-related species.

Notes and references

1 Y. Nabae, I. Yamanaka and K. Otsuka, *Appl. Catal., A*, 2005, **280**, 149.
2 G. Liu, X. G. Li, P. Ganesan and B. N. Popov, *Appl. Catal., B*, 2009, **93**, 156.
3 Y. J. Feng and N. Alonso-Vante, *Phys. Status Solidi B*, 2008, **245**, 1792.
4 R. Bashyam and P. Zelenay, *Nature*, 2006, **443**, 63.
5 M. Lefèvre, E. Proietti, F. Jaouen and J.-P. Dodelet, *Science*, 2009, **324**, 71.
6 C. W. B. Bezerra, L. Zhang, K. C. Lee, H. S. Liu, A. L. B. Marques, E. P. Marques, H. J. Wang and J. J. Zhang, *Electrochim. Acta*, 2008, **53**, 4937.
7 Z. Liu, H. Nie, Z. Yang, J. Zhang, Z. Jin, Y. Lu, Z. Xiao and S. Huang, *Nanoscale*, 2013, **5**, 3283.
8 L. Yang, S. Jiang, Y. Zhao, L. Zhu, S. Chen, X. Wang, Q. Wu, J. Ma, Y. Ma and Z. Hu, *Angew. Chem., Int. Ed.*, 2011, **50**, 7132.
9 Y. Gorlin and T. F. Jaramillo, *J. Am. Chem. Soc.*, 2010, **132**, 13612.
10 Z. S. Wu, S. B. Yang, Y. Sun, K. Parvez, X. L. Feng and K. Müllen, *J. Am. Chem. Soc.*, 2012, **134**, 9082.
11 D. S. Geng, H. Liu, Y. G. Chen, R. Y. Li, X. L. Sun, S. Y. Ye and S. Knights, *J. Power Sources*, 2011, **196**, 1795.
12 K. Parvez, S. B. Yang, Y. Hernandez, A. Winter, A. Turchanin, X. L. Feng and K. Müllen, *ACS Nano*, 2012, **6**, 9541.

13 X. Y. Yan, X. L. Tong, Y. F. Zhang, X. D. Han, Y. Y. Wang, G. Q. Jin, Y. Qin and X. Y. Guo, *Chem. Commun.*, 2012, **48**, 1892.
14 Y. Wang, X. J. Lu, Y. Liu and Y. Q. Deng, *Electrochem. Commun.*, 2013, **31**, 108.
15 F. Q. Kong, *Electrochim. Acta*, 2012, **68**, 198.
16 J. B. Xu, P. Gao and T. S. Zhao, *Energy Environ. Sci.*, 2012, **5**, 5333.
17 A. Restovic, E. Ríos, S. Barbato, J. Ortiz and J. L. Gautier, *J. Electroanal. Chem.*, 2002, **522**, 141.
18 Y. Y. Liang, Y. G. Li, H. L. Wang, J. G. Zhou, J. Wang, T. Regier and H. J. Dai, *Nat. Mater.*, 2011, **10**, 780.
19 J. B. Xu, P. Gao and T. S. Zhao, *Energy Environ. Sci.*, 2012, **5**, 5333.
20 A. L. M. Reddy, M. M. Shaijumon, S. R. Gowda and P. M. Ajayan, *Nano Lett.*, 2009, **9**, 1002.
21 H. Wang, R. Côté, G. Faubert, D. Guay and J. P. Dodelet, *J. Phys. Chem. B*, 1999, **103**, 2042.
22 Z. X. Wu, Y. Y. Lv, Y. Y. Xia, P. A. Webley and D. Y. Zhao, *J. Am. Chem. Soc.*, 2012, **134**, 2236.
23 J. Zhang, J.-O. Müller, W. Q. Zheng, D. Wang, D. S. Su and R. Schlögl, *Nano Lett.*, 2008, **8**, 2738.
24 X. Z. Cui, J. L. Shi, L. X. Zhang, M. L. Ruan and J. H. Gao, *Carbon*, 2009, **47**, 186.
25 Q. J. He, J. L. Shi, F. Chen, M. Zhu and L. X. Zhang, *Biomaterials*, 2010, **31**, 3335.
26 Z. L. Hua, J. Zhou and J. L. Shi, *Chem. Commun.*, 2011, **47**, 10536.
27 Y. S. Li, Y. Chen, L. Li, J. L. Gu, W. R. Zhao, L. Li and J. L. Shi, *Appl. Catal., A*, 2009, **366**, 57.
28 J. L. Shi, *Chem. Rev.*, 2013, **113**, 2139.
29 Z. S. Wu, W. C. Ren, L. Wen, L. B. Gao, J. P. Zhao, Z. P. Chen, Gu. M. Zhou, F. Li and H. M. Cheng, *ACS Nano*, 2010, **4**, 3187.
30 J. Feng, Y. Y. Liang, H. L. Wang, Y. G. Li, B. Zhang and J. G. Zhou, *Nano Res.*, 2012, **5**, 718.
31 Y. Wang, X. J. Lu, Y. Liu and Y. Q. Deng, *Electrochem. Commun.*, 2013, **31**, 108.
32 F. Kleitz, S. H. Choi and R. Ryoo, *Chem. Commun.*, 2003, 2136.
33 J. Sauer, F. Marlow, B. Spliethoff and F. Schüth, *Chem. Mater.*, 2002, **14**, 217.
34 H. Vidal, S. Bernal, R. T. Baker, D. Finol, J. A. Pérez Omil, J. M. Pintado and J. M. Rodriguez-lzquierdo, *J. Catal.*, 1999, **183**, 53.
35 M. R. Gao, Q. Gao, J. Jiang, C. H. Cui, W. T. Yao and S. H. Yu, *Angew. Chem., Int. Ed.*, 2011, **50**, 4905.
36 Y. J. Feng, T. He and N. Alonso-Vante, *Chem. Mater.*, 2008, **20**, 26.

